Physics Letters A 381 (2017) 2715–2720

Contents lists available at ScienceDirect

Physics Letters A

www.elsevier.com/locate/pla

Influence of different stoichiometric Cr-oxides created via oxygen ion-beam bombardment on the magnetism of the NiFe/Cr-oxide exchange-biased systems

Chao Zheng [a], Wen-Tzu Lo [b], Hsun-Feng Hsu [b], Yaroslav Wroczynskyj [c], Ko-Wei Lin [b,*], Johan van Lierop [c,*], Philip W.T. Pong [a,*]

[a] Department of Electrical and Electronic Engineering, The University of Hong Kong, Hong Kong
[b] Department of Materials Science and Engineering, National Chung Hsing University, Taichung 402, Taiwan
[c] Department of Physics and Astronomy, University of Manitoba, Winnipeg, MB, R3T 2N2, Canada

ARTICLE INFO

Article history:
Received 3 December 2016
Received in revised form 2 April 2017
Accepted 5 June 2017
Available online 8 June 2017
Communicated by M. Wu

Keywords:
Ion-beam bombardment
Cr-oxide
Exchange bias
Coercivity

ABSTRACT

In exchange-biased systems, antiferromagnetic Cr_2O_3 has drawn intensive attention because of its highly anisotropic structure. However, other Cr-oxide phases can be formed during fabrication. The influence of different stoichiometric Cr-oxides on the magnetism of the NiFe/Cr-oxide bilayers was studied. We find that paramagnetic CrO_3 grains could promote the formation of domain states in the Cr-oxide layer by magnetically isolating antiferromagnetic domains. These domain states gave rise to an excess of irreversible magnetic moments at the NiFe/Cr-oxide interface, causing a nontrivial increase in the exchange bias. The presence of ferromagnetic CrO_2 grains in the Cr-oxide layer introduced abundant magnetic disorders. These magnetic disorders acted as pinning sites and impeded the domain-wall motion, which resulted in an increase of the coercivity. These results indicate that the magnetism of the NiFe/Cr-oxide bilayers can be remarkably affected by different Cr-oxide phases, enabling control of both the coercivity and exchange bias and providing a possible route to improve the performance of exchange-biased devices.

1. Introduction

The exchange interaction between the ferromagnetic (FM) and antiferromagnetic (AF) layers results in a shift of the magnetic hysteresis loop of FM/AF bilayer systems, known as the exchange bias effect [1,2]. The exchange bias is crucial for the operation and performance of modern spintronic devices, such as magnetoresistive sensors [3,4] and spin torque oscillators [5,6]. In exchange-biased systems, the AF Cr_2O_3 has drawn intensive attention because of its highly anisotropic structure, which enables efficient control of its spin direction by altering its crystallographic orientation [7,8]. Other stoichiometric Cr-oxide phases can be formed during the fabrication process, which exhibit different structures and magnetic properties. The CrO_2 phase has a tetragonal rutile structure and is a ferromagnetic oxide with a relatively high Curie temperature of 398 K [9]. The orthorhombic CrO_3 phase is paramagnetic, which can decompose to the CrO_2 phase and finally convert to the most stable Cr_2O_3 phase by gradually losing its oxygen [10]. The formation of these metastable phases in the Cr-oxide layer can affect its magnetic properties, which consequently changes the magnetism of the FM/Cr-oxide exchange-bias systems. Previously, different Cr-oxide composites have been fabricated by mainly utilizing sintering [11], sputtering [12,13], and chemical vapor deposition [14] in order to investigate their structural or magnetic properties. In this work, a dual ion-beam bombardment technique [15] was used to deposit the Cr-oxide layer. Compared to the fabrication methods that were adopted in the literature, this technique can more conveniently change the type of the Cr-oxide compound by simply varying the O_2/Ar ratio during the deposition of the Cr-oxide layer. More importantly, the composition of the Cr-oxide layer has been reported to be impacted by the annealing effect in our previous study [16]. However, the influence of different stoichiometric Cr-oxides on the magnetism of the NiFe/Cr-oxide bilayers has not been discussed in detail, which is therefore investigated in this work.

In this work, the Cr-oxide layers containing different stoichiometric Cr-oxide phases were deposited on SiO_2 or Al_2O_3 substrates using the dual ion-beam bombardment. Different O_2/Ar ratios were used to alter the composition of the Cr-oxide layer. The microstruc-

* Corresponding authors.
E-mail addresses: kwlin@dragon.nchu.edu.tw (K.-W. Lin), johan@physics.umanitoba.ca (J. van Lierop), ppong@eee.hku.hk (P.W.T. Pong).

http://dx.doi.org/10.1016/j.physleta.2017.06.011
0375-9601/

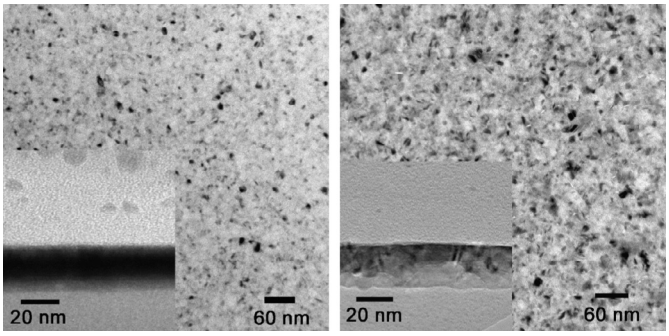

Fig. 1. Bright-field TEM images of the (a) as-deposited and (b) annealed NiFe/Cr-oxide (41% O_2/Ar)/SiO_2 samples, respectively. The insets are the corresponding cross-sectional TEM images.

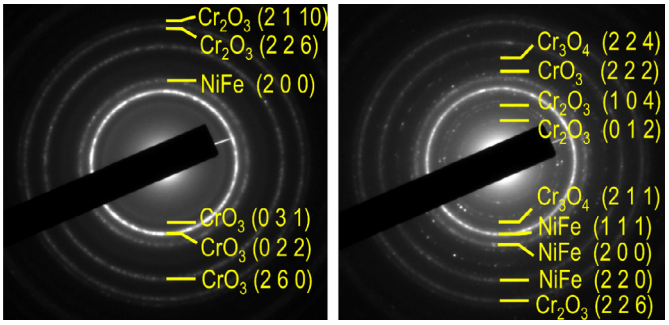

Fig. 2. Selected area electron diffraction (SAED) patterns of the (a) as-deposited and (b) annealed NiFe/Cr-oxide (41% O_2/Ar)/SiO_2 samples, respectively.

tural and magnetic properties of the Cr-oxide layers were found to be significantly affected by the annealing process, as well as by the substrate and O_2/Ar ratio, which consequently changes the magnetism of the NiFe/Cr-oxide bilayers.

2. Experimental methods

The NiFe/Cr-oxide bilayers were deposited on thermally oxidized Si(001) or single crystal Al(0001) substrates by utilizing a dual ion-beam deposition technique [17]. The base pressure of the process chamber was maintained at 4×10^{-5} Pa (3×10^{-7} Torr). A Kaufman source (800 V, 7.5 mA) was applied to sputter a commercial $Ni_{80}Fe_{20}$ (at.%) or Cr target. During deposition of the Cr layer, an End-Hall source with a mixture of O_2 and Ar (41% or 26% O_2/Ar) ion beam was directed towards the substrate to oxidize the Cr layer. The working pressure of the chamber was stabilized at 4×10^{-2} Pa (3×10^{-4} Torr) and no magnetic field was applied during deposition. The annealed samples were prepared by annealing the Cr-oxide layer at 700 °C at 4×10^{-5} Pa (3×10^{-7} Torr) for 10 min before deposition of the NiFe layer. The deposition rates of the Cr-oxide and NiFe layers were maintained at around 1.5 nm/min and 2.0 nm/min, respectively. During the deposition of both the NiFe and Cr-oxide layers, the substrate was left at ambient temperature. Both as-deposited and annealed NiFe/Cr-oxide bilayers with Cr-oxide thickness of 15 nm and NiFe thickness of 10 nm were prepared. Microstructural analysis was performed using a transmission electron microscope (TEM; JEOL JEM-2010) operating at 200 kV and surface morphology was characterized using an atomic force microscope (AFM; NT-MDT Slover Pro-M). X-ray diffraction (XRD) patterns were acquired using a Bruker D8 Discover with a CuK_α source operating at 50 kV, 30 mA. Low-temperature magnetic measurements were carried out in a superconducting quantum interference device (SQUID; Quantum Design MPMS) where a cooling field of 2 T (20 kOe) was applied parallel to the sample plane. The zero-field-cooled (ZFC) and field-cooled (FC) curves were measured with an in-plane magnetic field of 10 mT (100 Oe) over a temperature range from 400 K to 10 K.

3. Results and discussion

3.1. Influence of annealing effect

Microstructural properties of both the as-deposited and annealed NiFe/Cr-oxide (41% O_2/Ar)/SiO_2 samples were investigated via TEM. Figs. 1(a) and 1(b) show the bright-field TEM images for the as-deposited and annealed samples, which reveal a growth of the grain size after annealing. The increased grain size can be clearly identified as the large light-colored regions formed in the annealed sample, as exhibited in the inserted cross-sectional TEM images. Figs. 2(a) and 2(b) display the selected area electron diffraction (SAED) patterns for the as-deposited and annealed samples, respectively. For the fcc NiFe layer of the as-deposited sample, the estimated interplanar distance of the (2 0 0) planes is $d \sim 1.80$ Å and the corresponding lattice parameter is $a \sim 3.60$ Å, which is in agreement with that in the powder diffraction pattern database (PDF#47-14085/NiFe: $a \sim 3.592$ Å). The Cr_2O_3 and CrO_3 phases are identified in the as-deposited sample. For the hexagonal Cr_2O_3 phase, the interplanar distances of the (2 2 6) and (2 1 10) planes are $d \sim 1.09$ Å and ~1.04 Å, respectively. The lattice parameters for the Cr_2O_3 phase estimated from the SAED patterns are $a \sim 4.99$ Å and $c \sim 13.49$ Å. For the orthorhombic CrO_3 phase, the calculated interplanar distances of the (0 3 1), (0 2 2), and (2 6 0) planes are $d \sim 2.47$ Å, ~2.09 Å, and ~1.29 Å, respectively. The lattice parameters for the CrO_3 phase are $a \sim 5.59$ Å, $b \sim 8.64$ Å and $c \sim 4.76$ Å. For the annealed sample, the interplanar distances of the NiFe (1 1 1), (2 0 0), and (2 2 0) planes are $d \sim 2.08$ Å, ~1.80 Å, and ~1.27 Å, respectively. The NiFe lattice parameter is estimated to be $a \sim 3.60$ Å, which is the same as that of the as-deposited sample. The annealed Cr-oxide layer mainly consists of Cr_2O_3, CrO_3, and Cr_3O_4 phases. For the hexagonal Cr_2O_3 phase, the calculated interplanar distances of the (0 1 2), (1 0 4), and (2 2 6) planes are $d \sim 3.74$ Å, ~2.72 Å, and ~1.08 Å, respectively. The lattice parameters for the Cr_2O_3 phase estimated from the SAED patterns are $a \sim 5.14$ Å and $c \sim 13.75$ Å. For the tetragonal Cr_3O_4 phase, the calculated interplanar distances of the (2 1 1) and (2 2 4) planes are $d \sim 2.53$ Å and ~1.45 Å, respectively. The lattice parameters for the Cr_3O_4 phase are $a \sim 5.95$ Å and $c \sim 7.65$ Å. For both as-deposited and annealed samples, the calculated lattice parameters of the Cr-oxide phases are consistent with those reported in the powder diffraction pattern database (PDF#38-1479/Cr_2O_3: $a \sim 4.959$ Å, $c \sim 13.594$ Å; PDF#32-0285/CrO_3: $a \sim 5.749$ Å, $b \sim 8.556$ Å, $c \sim 4.796$ Å; PDF#12-0559/Cr_3O_4: $a \sim 6.145$ Å, $c \sim 7.550$ Å). The diffraction pattern corresponding to the CrO_3 phase became discontinuous and much dimmer after annealing treatment, which suggests a decreasing amount of the CrO_3 phase attributed to the thermal decomposition of CrO_3 to Cr_2O_3 [10]. The presence of the Cr_3O_4 phase suggests that Cr^{2+} valence states were formed in the annealed samples, because both Cr^{3+} and Cr^{2+} valence states existed in the Cr_3O_4 phase. These Cr^{2+} states probably arose from the Cr(3d)–O(2p) charge transfer process involved in the annealing process, resulting in a reduction in the valence state of Cr from Cr^{3+} to Cr^{2+} [18]. Furthermore, the presence of abundant bright diffraction spots in the SAED patterns of the annealed samples is consistent with the enlarged grains observed in the TEM images.

The surface morphology of the as-deposited and annealed NiFe/Cr-oxide (41% O_2/Ar)/SiO_2 samples was characterized using AFM, as shown in Fig. 3. Upon annealing the root-mean-square (RMS) roughness of the NiFe surface increased from 0.232 nm to

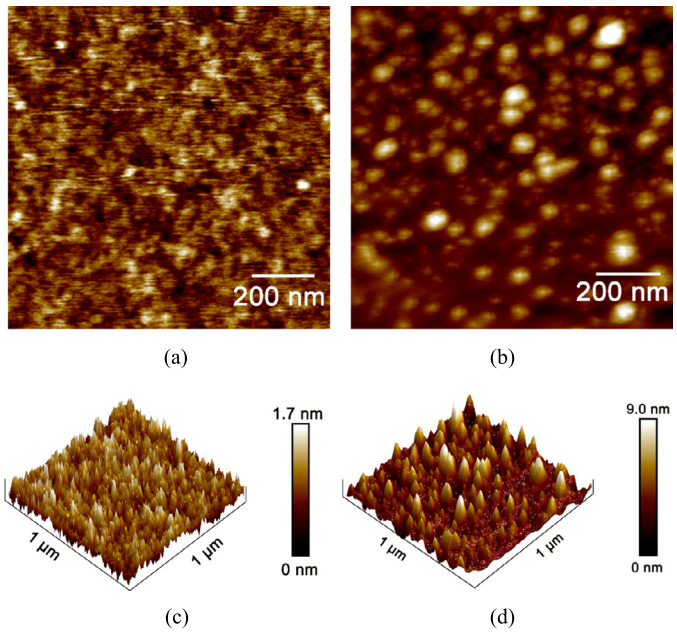

Fig. 3. 2D and 3D atomic force microscope (AFM) images of the (a, c) as-deposited and (b, d) annealed NiFe/Cr-oxide (41% O_2/Ar)/SiO_2 samples, respectively. The scanning area is 1 μm × 1 μm.

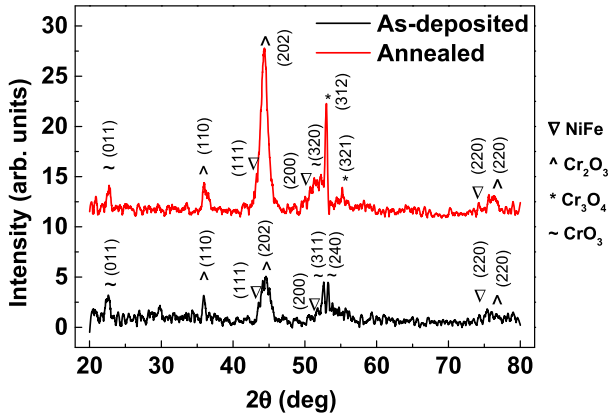

Fig. 4. X-ray diffraction (XRD) patterns of the as-deposited and annealed NiFe/Cr-oxide (41% O_2/Ar)/SiO_2 samples.

1.190 nm. Also, an increase of the grain size was exhibited after annealing, in line with the aforementioned TEM results.

XRD measurements were carried out to further investigate the influence of the annealing process on the microstructure of the NiFe/Cr-oxide bilayers, as shown in Fig. 4. The stoichiometric and microstructural properties of the Cr-oxide layers were strongly affected by the annealing process. After annealing, the peak intensity of the Cr_2O_3(202) orientation became much stronger accompanied by a decrease of the full width at half maximum (FWHM) from 1.39° to 1.06°. These phenomena indicate an improvement of the crystallinity and a growth of the Cr_2O_3 grains [19]. The preferred orientation of the CrO_3 phase was changed from (311) or (240) to (320) after annealing. Also, the AF Cr_3O_4 phase was identified in the annealed sample, which is consistent with the SAED results.

In order to determine the impact of annealing effect on the magnetic properties of the NiFe/Cr-oxide bilayers, hysteresis loops of the as-deposited and annealed samples were measured at 10 K, as shown in Fig. 5. Compared to the annealed NiFe/Cr-oxide bilayer, the as-deposited bilayer exhibited a notably larger exchange bias field of ~7.57 mT. As suggested by the bright CrO_3(031) ring in

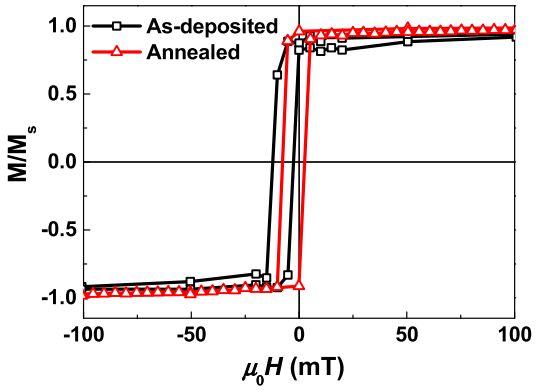

Fig. 5. Magnetic hysteresis loops of the as-deposited and annealed NiFe/Cr-oxide (41% O_2/Ar)/SiO_2 samples measured at 10 K. The measured magnetization (M) was normalized by the saturation field (M_s). The M vs H curves were measured at 10 K with a cooling field of 2 T (20 kOe) applied parallel to the sample plane.

the SAED patterns (Fig. 2a), the considerable amount of the paramagnetic CrO_3 phase formed in the as-deposited Cr-oxide layer is believed to be responsible for the relatively large exchange bias of the as-deposited sample. The paramagnetic CrO_3 phase promoted the formation of domain states in the AF Cr-oxide layer [20,21] by enabling the AF Cr-oxide domains to be magnetically separated, thus reducing the possibility of domain wall nucleation and growth amongst the AF domains (and altering the AF domain states) during the reversal process of the magnetization loop measurement. More specifically, these domain states gave rise to an excess of irreversible magnetic moments [22] at the NiFe/Cr-oxide interface, causing a nontrivial increase in the exchange bias. During the annealing process, a significant portion of the paramagnetic CrO_3 phase was thermally decomposed to the AF Cr_2O_3 phase, which hindered the formation of the domain states and substantially reduced the irreversible magnetic moments at the interface, leading to a decline in the exchange bias (as shown in Fig. 5).

The temperature dependence of the magnetization was measured under ZFC and FC over a temperature range from 400 K to 10 K, as shown in Fig. 6. For both the as-deposited and annealed samples, the FC magnetization continuously increases with decreasing temperature. The ZFC curve overlaps with the FC one above a critical temperature, which is known as the irreversibility temperature (T_{irr}) [23]. Upon further reduction in temperature, the ZFC magnetization begins to decrease and becomes more significant as temperature continues to decrease. Compared to the as-deposit samples, the ZFC curve for the annealed samples reveals a sharper drop at low temperature. This behavior is presumably attributed to the narrow distribution of the NiFe grain sizes in the annealed samples and similar energy barrier for each grain. As a result, magnetic moments for a large proportion of the grains are frozen during the cooling process, leading to a sudden drop in the ZFC magnetization [24].

3.2. Influence of O_2/Ar ratio

XRD measurements were conducted to investigate the microstructural properties of the NiFe/Cr-oxide bilayers with different O_2/Ar ratios, as shown in Fig. 7. For the NiFe/Cr-oxide (26% O_2/Ar)/SiO_2 samples, the Cr-oxide layer contains the CrO_2, Cr_2O_3, Cr_3O_4 and CrO_3 phases. The CrO_2 phase is metastable and can decompose into the more stable Cr_2O_3 phase during the annealing process [10]. However, the decomposition process is relatively slow and the complete transformation requires an annealing temperature above 700 °C [25,26]. In our case, the annealing temperature and duration are 700 °C and 10 min, therefore the decomposition

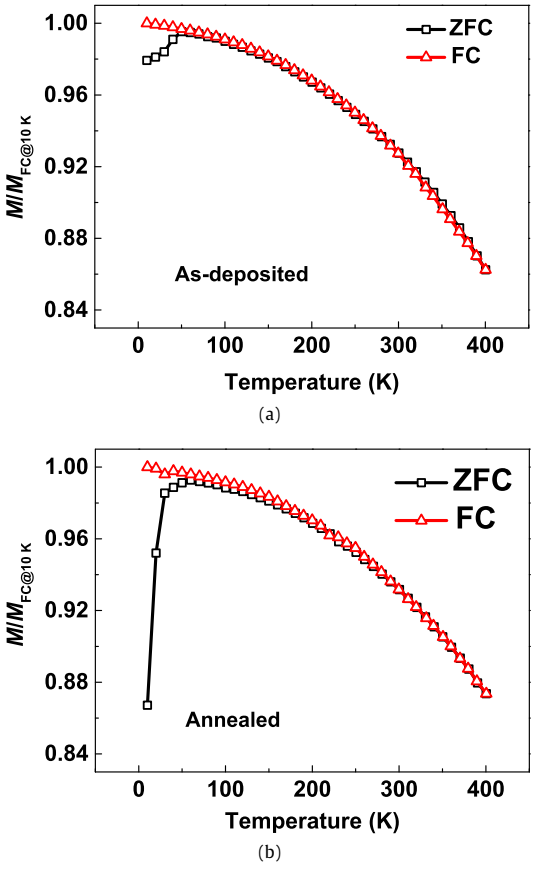

Fig. 6. Zero-field-cooled (ZFC) and field-cooled (FC) curves for the (a) as-deposited and (b) annealed NiFe/Cr-oxide (41% O_2/Ar)/SiO_2 samples, respectively. These ZFC and FC curves were measured in an in-plane magnetic field of 10 mT (100 Oe) over a temperature range from 400 K to 10 K. The measured magnetization (M) was normalized by the FC magnetization at 10 K ($M_{FC@10\,K}$). The M vs H curves were measured at 10 K with a cooling field of 2 T (20 kOe) applied parallel to the sample plane.

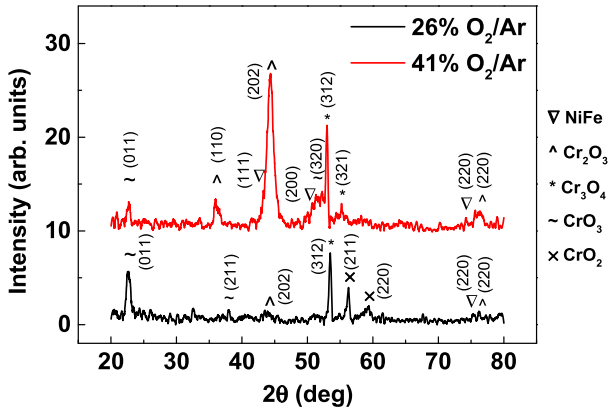

Fig. 7. X-ray diffraction (XRD) patterns of the annealed NiFe/Cr-oxide (26% O_2/Ar)/SiO_2 and NiFe/Cr-oxide (41% O_2/Ar)/SiO_2 samples.

of the CrO_2 phase was likely not completed. As a result, a certain amount of the CrO_2 phase still existed after annealing and its corresponding diffraction peaks exhibited in the XRD spectrum (as shown in Fig. 7). Upon increasing the ratio of the O_2/Ar mixture from 26% to 41% during the deposition of the Cr-oxide layer, intensity of the Cr_2O_3(202) peak showed a remarkable rise and the Cr_2O_3(110) peak became observable, suggesting that other Cr-oxide phases transformed to the more stable Cr_2O_3 phase.

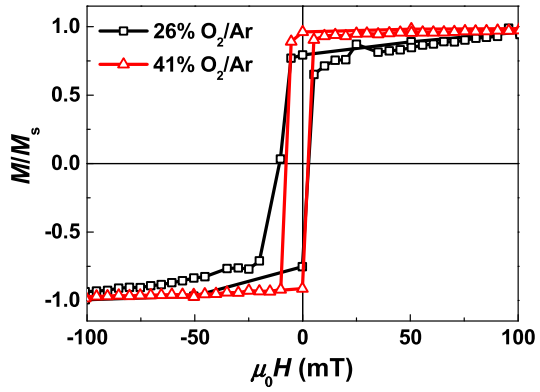

Fig. 8. Magnetic hysteresis loops of the annealed NiFe/Cr-oxide (26% O_2/Ar)/SiO_2 and NiFe/Cr-oxide (41% O_2/Ar)/SiO_2 samples measured at 10 K. The measured magnetization (M) was normalized by the saturation field (M_s).

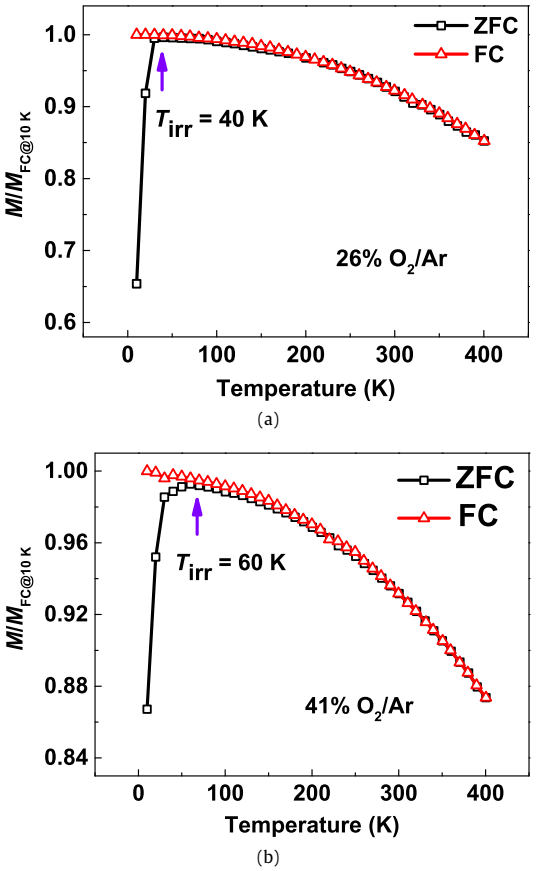

Fig. 9. Zero-field-cooled (ZFC) and field-cooled (FC) curves for the annealed (a) NiFe/Cr-oxide (26% O_2/Ar)/SiO_2 and (b) NiFe/Cr-oxide (41% O_2/Ar)/SiO_2 samples, respectively. The measured magnetization (M) was normalized by the FC magnetization at 10 K ($M_{FC@10\,K}$). The M vs H curves were measured at 10 K with a cooling field of 2 T (20 kOe) applied parallel to the sample plane.

The altered composition of the Cr-oxide layer strongly affected the magnetic properties of the NiFe/Cr-oxide thin films. Fig. 8 shows hysteresis loops of the samples measured at 10 K. Compared to the samples deposited with higher O_2/Ar ratio, the NiFe/Cr-oxide (26% O_2/Ar)/SiO_2 samples exhibited a relatively larger coercivity of 6.44 mT. The enhancement of the coercivity was likely due to the existence of the FM CrO_2 phase in the Cr-oxide layer. The FM spins in the CrO_2 grains could be pinned by AFM spins and consequently boosted the coercivity of the NiFe/Cr-oxide bilayers [27–29]. Figs. 9(a) and 9(b) demonstrate the ZFC and FC magne-

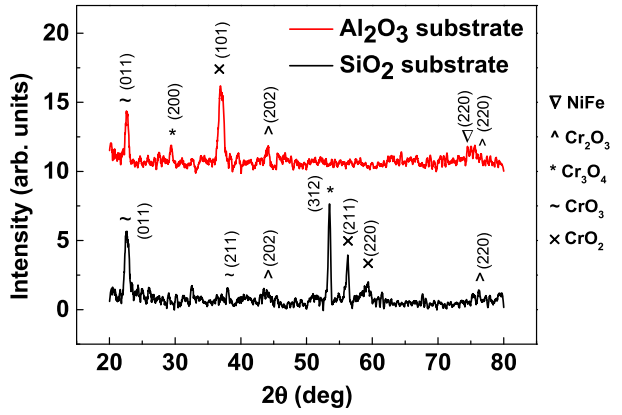

Fig. 10. X-ray diffraction (XRD) patterns of the annealed NiFe/Cr-oxide (26% O_2/Ar) deposited on the SiO_2 and Al_2O_3(0001) substrates.

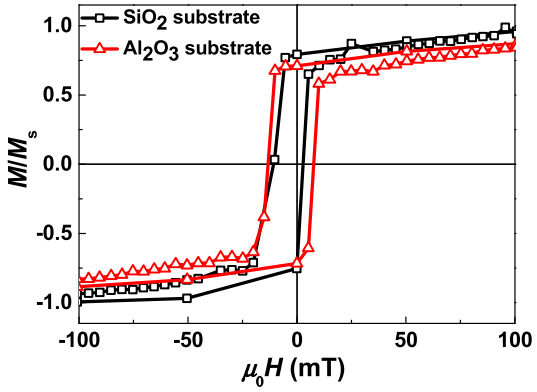

Fig. 11. Magnetic hysteresis loops of the annealed NiFe/Cr-oxide (26% O_2/Ar) deposited on the SiO_2 and Al_2O_3 (0001) substrates. The measured magnetization (M) is normalized by the saturation field (M_s).

tizations of the NiFe/Cr-oxide (26% O_2/Ar)/SiO_2 and NiFe/Cr-oxide (41% O_2/Ar) /SiO_2 samples, respectively. The NiFe/Cr-oxide (41% O_2/Ar) bilayers show a board peak in the ZFC curve. This behavior indicates that the distribution of the NiFe grain sizes became wider upon increasing the O_2/Ar ratio, which induced a wider distribution of the blocking temperatures. In addition, the wider distribution of the NiFe grain sizes could also lead to a rise of T_{irr} that represents the blocking temperature of the grains with largest energy barrier [24], which is consistent with the measured results that T_{irr} increases from 40 K to 60 K.

3.3. *Influence of substrate material*

The influence of the substrate material on the microstructure of the NiFe/Cr-oxide bilayers was also studied, as shown in Fig. 10. After replacing the amorphous SiO_2 substrates with the single crystal Al_2O_3 (0 0 0 1) ones, the preferred orientation of the Cr_3O_4 grains changed from (3 1 2) to (2 0 0) while that of the CrO_2 grains shifted from (2 1 1) to (1 0 1). Furthermore, the FWHM value of the peak for the CrO_3 grains decreased from around 0.65° (0 1 1) to 0.51° (0 1 1), indicating the improved crystallinity of the CrO_3 grain in the samples prepared using the Al_2O_3 substrates. The improved crystallinity of the CrO_3 phase is attributed to the closely matched lattice parameters between the c-axis (PDF#32-0285: $c = 0.47961$ nm) of the CrO_3 phase and a-axis (PDF#46-1212: $a = 0.47587$ nm) of the Al_2O_3 (0 0 0 1). However, the FWHM value of the peak for the CrO_2 grains increased from around 0.41° (2 1 1) to 0.84° (1 0 1), suggesting that the crystallinity of the CrO_2 grain was degraded after replacing the SiO_2 substrates with the Al_2O_3 substrates. The different crystal structures of the tetragonal CrO_2 and hexagonal Al_2O_3 (0 0 0 1) can lead to imperfect textures in the CrO_2 phase, giving rise to a degradation of CrO_2 crystallinity [30].

The magnetic properties of the NiFe/Cr-oxide (26% O_2/Ar) bilayers deposited on both SiO_2 and Al_2O_3 (0 0 0 1) substrates were investigated, as shown in Fig. 11. After using the Al_2O_3 substrates, the coercivity was further raised from 6.44 mT to 10.16 mT. The increased coercivity probably originated from the formation of more magnetic disorders in the Cr-oxide layer induced by the degraded crystallinity of the FM CrO_2 grains, as suggested by the increased FWHM value of the CrO_2 peaks. These magnetic disorders can act as pinning centers and impede the domain-wall motion during the magnetic reversal, resulting in an enhanced coercivity [27,29].

4. Conclusions

In this work, the influence of different stoichiometric Cr-oxides on the magnetism of the NiFe/Cr-oxide exchange-biased systems was investigated. The composition and magnetic properties of the Cr-oxide layer can be notably altered by the annealing effect, as well as by the ratio of the O_2/Ar mixture and the type of substrate. The paramagnetic CrO_3 phase facilitated the formation of domain states in the AF Cr-oxide layer by magnetically isolating antiferromagnetic domains. As a result, the possibility of domain wall nucleation and growth amongst the AF domains was reduced and the AF domain states were altered during the reversal process of the magnetization loop measurement. These domain states could introduced an excess of irreversible magnetic moments at the NiFe/Cr-oxide interface, leading to a nontrivial enhancement of the exchange bias. However, the FM CrO_2 grains were formed in the Cr-oxide layer by altering the ratio of O_2/Ar mixture and changing the type of substrate. The FM spins in the CrO_2 grains can be pinned by AFM spins, which hindered the domain-wall motion during the magnetic reversal, resulting in an enhanced coercivity. These results indicate that the magnetism of the NiFe/Cr-oxide bilayers can be remarkably affected by different stoichiometric Cr-oxides, enabling control of both the exchange bias and coercivity and offering a promising route to improve the performance of the modern spintronic devices.

Acknowledgements

This work was supported in part by the MOST of Taiwan, the NSERC of Canada, and the Seed Funding Program for Basic Research and Small Project Funding Program from the University of Hong Kong, ITF Tier 3 funding (ITS/104/13, ITS/214/14), and University Grants Committee of Hong Kong (Contract No. AoE/P-04/08).

References

[1] J. Nogués, L. Morellon, C. Leighton, M.R. Ibarra, I.K. Schuller, Antiferromagnetic spin flop and exchange bias, Phys. Rev. B 61 (2000) R6455.
[2] G. Scholten, K.-D. Usadel, U. Nowak, Coercivity and exchange bias of ferromagnetic/antiferromagnetic multilayers, Phys. Rev. B 71 (2005) 064413.
[3] T. Scheike, H. Sukegawa, T. Furubayashi, Z. Wen, K. Inomata, T. Ohkubo, K. Hono, S. Mitani, Lattice-matched magnetic tunnel junctions using a Heusler alloy Co_2FeAl and a cation-disorder spinel Mg–Al–O barrier, Appl. Phys. Lett. 105 (2014) 242407.
[4] H. Kaiju, M. Takei, T. Misawa, T. Nagahama, J. Nishii, G. Xiao, Large magnetocapacitance effect in magnetic tunnel junctions based on Debye–Fröhlich model, Appl. Phys. Lett. 107 (2015) 132405.
[5] D. Houssameddine, U. Ebels, B. Delaët, B. Rodmacq, I. Firastrau, F. Ponthenier, B. Brunet, C. Thirion, J.-P. Michel, L. Prejbeanu-Buda, M.-C. Cyrille, O. Redon, B. Dieny, Spin-torque oscillator using a perpendicular polarizer and a planar free layer, Nat. Mater. 6 (2007) 447.
[6] H. Kubota, K. Yakushiji, A. Fukushima, S. Tamaru, M. Konoto, T. Nozaki, S. Ishibashi, T. Saruya, S. Yuasa, T. Taniguchi, Spin-torque oscillator based on magnetic tunnel junction with a perpendicularly magnetized free layer and in-plane magnetized polarizer, Appl. Phys. Express 6 (2013) 103003.

[7] Y. Shiratsuchi, T. Nakatani, R. Nakatani, M. Yamamoto, Superparamagnetism of ultrathin Co film on antiferromagnetic Cr_2O_3 layer, Inst. Phys. Conf. Ser. 165 (2009) 012034.
[8] J. Dho, M.G. Blamire, E.O. Chi, Correlation of the exchange interaction in $Ni_{81}Fe_{19}/Cr_2O_3$ bilayers with the antiferromagnetic spin configuration, Phys. Rev. B 72 (2005) 224421.
[9] J.J. Yuan, G.H. Wen, Y.B. Fan, C.P. Zhang, Q. Zhao, Z. Yin, X.K. Zhang, H.J. Yu, X.R. Zhu, Y.M. Xie, Preparation and magnetoresistance of submicron CrO_2 thin film on poly-crystal SnO_2 film, Physica B 477 (2015) 29–32.
[10] N.J.C. Ingle, R.H. Hammond, M.R. Beasley, Growth of the Cr oxides via oxygen reactive molecular beam epitaxy: comparison of the Mo and W oxides, J. Appl. Phys. 89 (2001) 4631–4635.
[11] P.Z. Si, H.X. Wang, W. Jiang, J.G. Lee, C.J. Choi, J.J. Liu, Synthesis, structure and exchange bias in $Cr_2O_3/CrO_2/Cr_2O_5$ particles, Thin Solid Films 519 (2011) 8423–8425.
[12] T. Ashida, Y. Sato, T. Nozaki, M. Sahashi, Effect of the Pt buffer layer on perpendicular exchange bias based on collinear/non-collinear coupling in a Cr_2O_3/Co_3Pt interface, J. Appl. Phys. 113 (2013) 17D711.
[13] Y. Shiratsuchi, H. Noutomi, H. Oikawa, T. Nakamura, M. Suzuki, T. Fujita, K. Arakawa, Y. Takechi, H. Mori, T. Kinoshita, M. Yamamoto, R. Nakatani, Detection and in situ switching of unreversed interfacial antiferromagnetic spins in a perpendicular-exchange-biased system, Phys. Rev. Lett. 109 (2012) 077202.
[14] R. Cheng, B. Xu, C.N. Borca, A. Sokolov, C.-S. Yang, L. Yuan, S.-H. Liou, B. Doudin, P.A. Dowben, Characterization of the native Cr_2O_3 oxide surface of CrO_2, Appl. Phys. Lett. 79 (2001) 3122–3124.
[15] S.K. Pandey, S.K. Pandey, C. Mukherjee, P. Mishra, M. Gupta, S.R. Barman, S.W. D'Souza, S. Mukherjee, Effect of growth temperature on structural, electrical and optical properties of dual ion beam sputtered ZnO thin films, J. Mater. Sci., Mater. Electron. 24 (2013) 2541–2547.
[16] K.-W. Lin, J.-Y. Guo, Tuning in-plane and out-of-plane exchange biases in $Ni_{80}Fe_{20}$/Cr-oxide bilayers, J. Appl. Phys. 104 (2008) 123913.
[17] L. Thomé, A. Debelle, F. Garrido, P. Trocellier, Y. Serruys, G. Velisa, S. Miro, Combined effects of nuclear and electronic energy losses in solids irradiated with a dual-ion beam, Appl. Phys. Lett. 102 (2013) 141906.
[18] A. Singhal, Study of electronic and magnetic properties of vacuum annealed Cr doped ZnO, J. Alloys Compd. 515 (2012) 12–15.
[19] A. Hayashi, K. Noi, N. Tanibata, M. Nagao, M. Tatsumisago, High sodium ion conductivity of glass–ceramic electrolytes with cubic Na_3PS_4, J. Power Sources 258 (2014) 420–423.
[20] P. Miltényi, M. Gierlings, J. Keller, B. Beschoten, G. Güntherodt, U. Nowak, K.D. Usadel, Diluted antiferromagnets in exchange bias: proof of the domain state model, Phys. Rev. Lett. 84 (2000) 4224–4227.
[21] U. Nowak, K.D. Usadel, J. Keller, P. Miltényi, B. Beschoten, G. Güntherodt, Domain state model for exchange bias, I: theory, Phys. Rev. B 66 (2002) 014430.
[22] J. Keller, P. Miltényi, B. Beschoten, G. Güntherodt, U. Nowak, K.-D. Usadel, Domain state model for exchange bias, II: experiments, Phys. Rev. B 66 (2002) 014431.
[23] A. Ahlawat, S. Satapathy, S. Bhartiya, M.K. Singh, R.J. Choudhary, P.K. Gupta, $BiFeO_3$/poly(methyl methacrylate) nanocomposite films: a study on magnetic and dielectric properties, Appl. Phys. Lett. 104 (2014) 042902.
[24] J. Jacob, M. Abdul Khadar, VSM and Mössbauer study of nanostructured hematite, J. Magn. Magn. Mater. 322 (2010) 614–621.
[25] D. Li, Z. Han, J. Zheng, X. Wang, D. Geng, J. Li, Z.D. Zhang, Spin canting and spin-flop transition in antiferromagnetic Cr_2O_3 nanocrystals, J. Appl. Phys. 106 (2009) 053913.
[26] M. Maciejewski, K. Köhler, H. Schneider, A. Baiker, Interconversion of CrO_2 formed by decomposition of chromium (III) nitrate nonahydrate, J. Solid State Chem. 119 (1995) 13–23.
[27] J. Spray, U. Nowak, Exchange bias in ferromagnetic/antiferromagnetic bilayers with imperfect interfaces, J. Phys. D, Appl. Phys. 39 (2006) 4536–4539.
[28] M. Ali, C.H. Marrows, B.J. Hickey, Controlled enhancement or suppression of exchange biasing using impurity δ layers, Phys. Rev. B 77 (2008) 134401.
[29] C. Leighton, J. Nogués, B. Jönsson-Åkerman, I.K. Schuller, Coercivity enhancement in exchange biased systems driven by interfacial magnetic frustration, Phys. Rev. Lett. 84 (2000) 3466–3469.
[30] M. Anwar, F. Czeschka, M. Hesselberth, M. Porcu, J. Aarts, Long-range supercurrents through half-metallic ferromagnetic CrO_2, Phys. Rev. B 82 (2010) 100501.